Enhancing the accuracy of seeding operation monitoring by seeding monitoring system based on flexible pressure sensors and SFIA

Yuxing Song[1], Jianguang Gong[2], Rui Zhao[3], Yongjun Wang[4], Xiaogeng Wang[1], Mingzhuo Guo[1*], Jiale Zhao[2,5*]

(1. *College of Biological and Agricultural Engineering, Jilin University, Changchun 130025, China*;
2. *State Key Laboratory of Smart Farm Technologies and Systems, Harbin 150036, China*;
3. *Beidahuang Information Co., Ltd., Harbin 150020, China*;
4. *College of Plant Science, Jilin University, Changchun 130062, China*;
5. *Key Laboratory of Bionics Engineering, Ministry of Education, Jilin University, Changchun 130025, China*)

Abstract: Conventional seeding monitors often exhibit diminished accuracy under challenging field conditions. To address this, this study introduces a novel monitoring system leveraging flexible pressure sensors integrated with a finger-clamp seed metering device. The core principle is that the passage of each seed-clamping finger over the seed outlet generates a distinct, continuous pressure signal profile. A sophisticated Signal Feature Identification Algorithm (SFIA) was developed that transforms this raw signal data into a one-dimensional image for analysis. By employing binarization and bilateral filtering, the SFIA effectively suppresses noise from field vibrations and extracts key topographical features, enabling precise quantification of seeding events through peak detection. The complete system, implemented using LabVIEW and Python, was rigorously evaluated in field trials. Under conventional tillage, the system achieved an overall monitoring accuracy of 96.55%, with reseeding and missed seeding detection accuracies of 98.96% and 98.55%, respectively. Critically, it maintained high performance in challenging no-till conditions, demonstrating 95.46% overall accuracy, with 98.35% for reseeding and 98.42% for missed seeding detection. This research validates a pressure-based sensing approach as a robust alternative to traditional methods, presenting a new technological pathway for developing high-precision seeding monitoring systems resilient to common agricultural interferences.

Keywords: seeding monitoring, pressure sensor, signal processing, feature extraction, no-till seeding
DOI: 10.25165/j.ijabe.20261903.10124

Citation: Song Y X, Gong J G, Zhao R, Wang Y J, Wang X G, Guo M Z, et al. Enhancing the accuracy of seeding operation monitoring by seeding monitoring system based on flexible pressure sensors and SFIA. Int J Agric & Biol Eng, 2026; 19(3): 225–234.

1 Introduction

Precision agriculture represents a cornerstone of modern farming, aiming to optimize crop yields and resource efficiency through data-driven management. Within this paradigm, the quality of seed placement is a foundational determinant of final crop stand, uniformity, and overall productivity[1,2]. Consequently, the development of robust, real-time seeding monitoring systems is crucial for achieving the full potential of precision planting operations. The predominant technology for this purpose relies on photoelectric sensors positioned at the seed tube outlet, which identify seeding events by detecting interruptions in a light beam. However, the efficacy of these optical systems is notoriously compromised in typical field environments. Airborne dust, debris, and high humidity can obstruct or scatter the light beam, degrading signal integrity and leading to monitoring inaccuracies that often fall below 92%. Such failures can result in significant annual crop losses, estimated as high as 234.8 kg/hm^2[3-5], underscoring the urgent need for a more resilient monitoring technology to enhance agricultural profitability and sustainability.

In response to the limitations of optical methods, mechanical sensing approaches, such as those using strain or pressure sensors, have emerged as a promising alternative. Because they rely on mechanical signals rather than light, they are inherently more robust against environmental interferents like dust and humidity[6-8]. These sensors are typically integrated directly into the seed metering mechanism, creating a self-contained mechanical system where the signal characteristics remain largely stable even when subjected to external vibrations. For instance, a system developed by Gierz et al.[9] using PVDF piezoelectric films demonstrated a monitoring accuracy of up to 94%, showcasing the potential of this modality. However, a critical bottleneck has hindered the application of strain-based sensors in high-fidelity precision seeding: the inability to reliably distinguish between single, multiple, or missed seeding events. Traditional monitoring systems employ simple threshold-based algorithms designed for discrete, binary (0/1) signals

Received date: 2025-08-28 **Accepted date:** 2026-04-10
Biographies: Yuxing Song, M.S., research interest: intelligent control systems for agricultural machinery, Email: songyuxing83817@outlook.com; **Jianguang Gong**, PhD, Professor, research interest: agricultural information technology, Email: gjg@hrbeu.edu.cn; **Rui Zhao**, Researcher, research interest: design of agricultural machinery, Email: 1210323410@qq.com; **Yongjun Wang**, PhD, Professor, research interest: crop cultivation physiology and sustainable production, Email: yjwang2026@jlu.edu.cn; **Xiaogeng Wang**, PhD, research interest: intelligent agricultural machinery systems, Email: xgwang@jlu.edu.cn.
***Corresponding author: Mingzhuo Guo**, PhD, Associate Professor, research interest: bionic intelligent agricultural machinery. Jilin University, Changchun 130022, China. Tel: +86-18504311293, Email: gmz@jlu.edu.cn; **Jiale Zhao**, PhD, Professor, research interest: intelligent agricultural machinery. Jilin University, Changchun 130022, China. Tel: +86-18843165417, Email: zhaojl@jlu.edu.cn.

generated by photoelectric sensors[10,11]. When multiple seeds pass in close succession, they often generate a single, prolonged signal interruption that these algorithms cannot resolve into individual events[12]. Strain sensors, in contrast, produce a continuous, analog time-series signal, rendering traditional thresholding methods fundamentally incompatible. This fundamental difference in signal type is the core reason why established algorithms are unsuitable for strain-based monitoring systems[13,14]. Therefore, unlocking the potential of mechanical sensing for precision applications necessitates the development of novel algorithms capable of interpreting the complex characteristics of these continuous signals[15,16].

Recent advancements in signal processing and image feature recognition provide a powerful new toolkit to address this challenge[17-19]. The central hypothesis in this study is that the continuous pressure signal, generated as a seed-laden finger-clamp passes over the sensor's active area, can be transformed and analyzed as a one-dimensional topographical image. Within this "image", the passage of each seed creates a distinct peak, or "trend", whose characteristics reflect the seeding status[20]. By leveraging sophisticated image processing algorithms, such as binarization for feature enhancement and bilateral filtering for high-precision noise reduction, it becomes possible to effectively isolate and count these peaks[21-23]. This signal-to-image approach offers a pathway to accurately quantify seeding events, even amidst the noise and vibrations inherent to field operations.

Building on this premise, this study introduces a novel seeding monitoring system that integrates flexible pressure sensors with a specially developed Signal Feature Identification Algorithm (SFIA). The core contribution lies in the development and validation of the SFIA, which is engineered to denoise raw pressure signals and accurately identify seeding-related features by treating them as image contours. We detail the design and implementation of the complete system, which was realized using LabVIEW and Python. To rigorously assess its performance, we conducted comprehensive field experiments comparing our system against conventional monitors under both standard conventional tillage and more challenging no-till conditions. This research thus provides a validated new approach for high-precision seeding monitoring, offering the algorithms, data, and principles to support the next generation of robust agricultural sensing technologies.

2 Materials and methods

2.1 Overall design of pressure-based seed sowing system

2.1.1 System operating scenario

The monitoring system is engineered specifically for the finger-clamp seed metering device, a prevalent technology in the northeastern agricultural regions of China. Its operational principle involves a series of articulated 'fingers' that apply continuous, directed pressure along the z-axis to convey individual seeds towards the seeding outlet, completing a seeding cycle. A key design feature is the biomimetic, fingertip-like structure of the clamps. This design constrains the seed, minimizing lateral displacement and ensuring the consistent application of downward pressure onto the seed guide mechanism's surface. This inherent stability is fundamental to generating a reliable and repeatable pressure signal for each seeding event.

To quantify this pressure for sensor selection, a static and dynamic force analysis, detailed in Equations (1)-(5), was conducted [24-26]. The analysis determined that the pressure exerted by a seed-laden finger on the guide surface consistently falls within a 0.05 to 0.2 MPa range. This predictable stress range directly informed the selection of an appropriate sensing element: a piezoelectric thin-film strain sensor (FSR, Shanghai Chengke Electronics Technology Co., Ltd., DF9-40 film strain sensor. Range: 2g-500g, trigger point: 1g.) from i-Motion (see Table 1 for specifications), which is highly sensitive within this operational pressure window. Consequently, by strategically positioning the FSR at the terminal point of the seed guide mechanism, the system is able to capture these stable, real-time pressure signals, effectively translating the mechanical action of each seeding event into a quantifiable electronic signal.

Table 1 Sensor parameters

Properties	Range	Properties	Range
sensor range	5-200 g	response time	5 ms
sensor thickness	0.1 mm	pressure resolution	1 g
substrate type	polyester	usage count	one million times

$$\begin{cases} \sum F_x = 0,\ f_2 + G\cos\theta_0 - F_a = 0 \\ \sum F_y = 0,\ f_1 - G\sin\theta_0 - J = 0 \\ \sum F_z = 0,\ F_i - F_n = 0 \\ \sum M_Q = 0,\ F_h a - F_i b = 0 \end{cases} \tag{1}$$

$$F_h = \sqrt{G^2 + J^2 f_2^2} \tag{2}$$

$$F_p = \sqrt{F_a^2 + f_1^2} = \sqrt{G^2 + J^2 + f_2^2 + 2G(f^2\cos\theta_0 + J\sin\theta_0)} \tag{3}$$

$$F_i = \frac{F_h a}{b} \tag{4}$$

$$\sigma_i = \frac{F_i}{A_i} \tag{5}$$

where, f_1, f_2 are friction force exerted by the seed metering device on the seed, N; G is gravitational force acting on the seed (seed gravity), N; F_a is thrust force applied by the finger clamp, N; J is centrifugal force acting on the seed due to rotation, N; F_i is clamping force applied by the finger, N; F_n is normal support force on the seed in z-axis direction, N; F_h is the resultant force vector combining G, J, and f_2, N; F_p is the resultant force vector combining F_a and f_1, N; θ_0 is the angle between the centrifugal force and gravity vectors, rad; a is the distance from the point of clamping force application to the resultant force F_h, m; b is the distance from the point of force application to the center of the stably clamped seed, m; σ_i is the stress exerted by the seed onto the surface of the seed guide mechanism, MPa; A_i is the contact area between the seed and the seed guide mechanism, m^2.

2.1.2 System composition and working principle

The pressure-based seeding monitoring system is architecturally divided into two primary, interconnected subsystems: a hardware-based signal acquisition system and a software-based signal feature recognition system (Figure 1a). The Signal Acquisition System comprises a piezoelectric thin-film strain sensor (FSR), a custom detection and differential amplification circuit, an NI signal acquisition card (USB-6003), and an industrial computer (IPC). Its function is to capture the raw pressure-induced electrical signals and convert them into a digital format for processing. The Signal Feature Recognition System is implemented using a combination of Python and LabVIEW. Python hosts the core Signal Feature Identification Algorithm (SFIA), while LabVIEW provides the user interface, real-time status display, and data storage module. Seamless data exchange between these two software environments is achieved via the integrated Python Node module in LabVIEW, creating a cohesive system for signal processing and analysis (Figure 1b).

The system's working principle follows a sequential process from signal generation to classification (Figure 2b). It begins when a seed-laden finger passes over the FSR sensor mounted at the seed guide outlet. This action induces a characteristic pressure change, resulting in a transient electrical signal whose amplitude profile initially increases and then decreases, forming a distinct peak as the

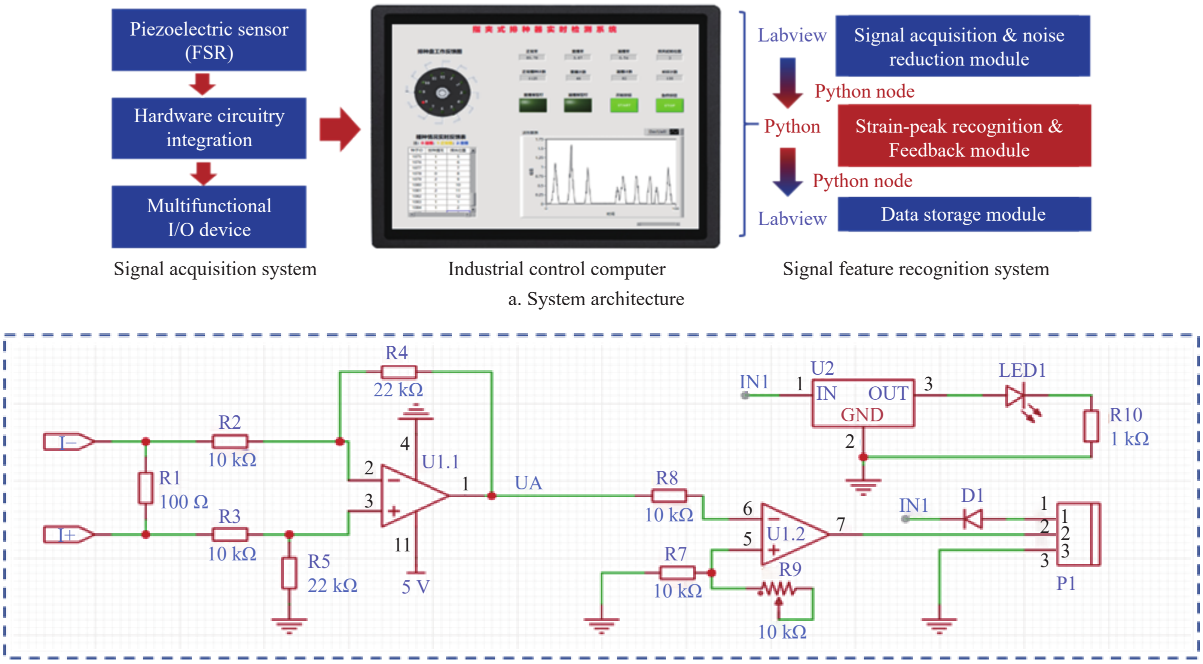

a. System architecture

b. System hardware circuitry

Figure 1 Corn precision seeding monitoring system based on SFIA algorithm

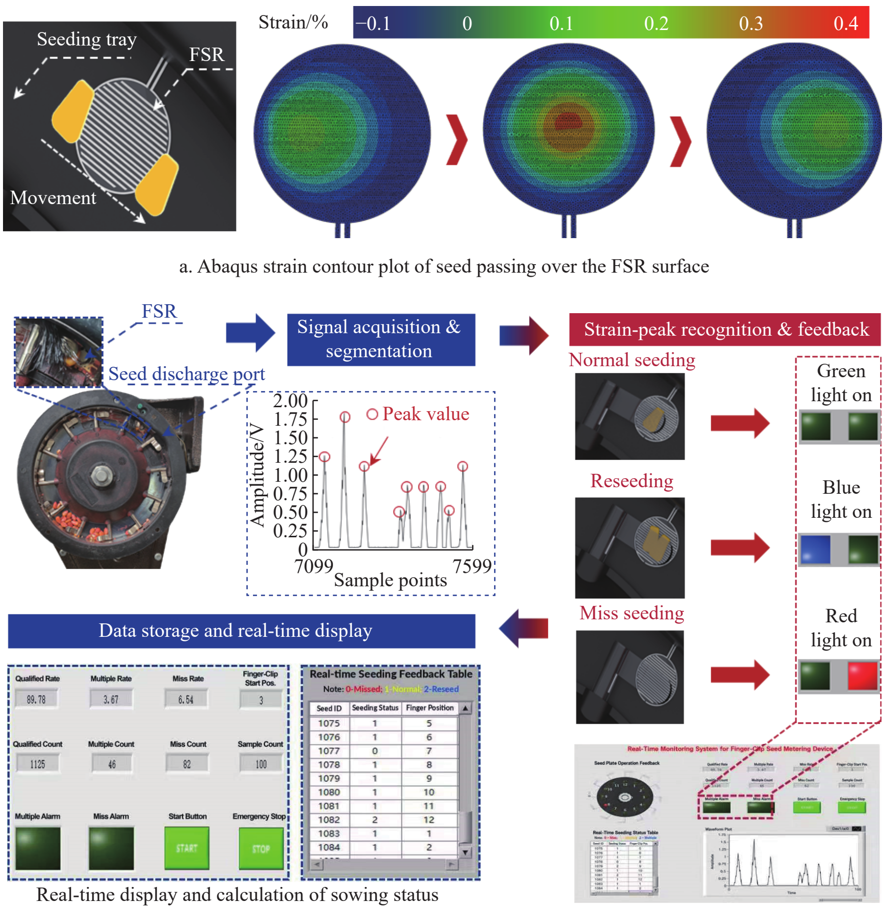

a. Abaqus strain contour plot of seed passing over the FSR surface

b. Working process of the strain-based seeding monitoring system

Figure 2 Working principle of the corn precision seeding monitoring system based on SFIA algorithm seed traverses the sensor's center (Figure 2a). The Signal Acquisition System captures this analog signal, which is then passed to the Signal Feature Recognition System. Here, the signal extraction module first converts the time-series dataset into a one-dimensional feature image. The core of the system's logic lies in quantifying the number of local extrema (peaks) within this image. The seeding status is determined by a direct mapping: zero peaks correspond to a missed seeding event, a single peak indicates a normal single seeding, and the presence of multiple peaks within a single seeding interval signifies a reseeding event. The SFIA further refines this by calculating the time intervals between detected peaks to ensure precise differentiation between single and multiple seeding events. Finally, the data storage module logs each classification result and continuously computes the overall seeding accuracy statistics in real time.

2.2 Sowing signal strain feature recognition algorithm

The successful translation of raw, noisy pressure data into discrete, actionable seeding classifications hinges upon a sophisticated computational framework. To this end, we developed a multi-stage Signal Feature Identification Algorithm (SFIA), engineered to systematically deconstruct and interpret the sensor's output. The foundational innovation of the SFIA is its paradigm of treating the one-dimensional, temporal pressure signal as a two-dimensional, spatial image. This transformation is pivotal, as it unlocks the vast and mature arsenal of computer vision and image processing techniques for what is fundamentally a signal analysis problem. The core of the SFIA is structured as a sequential processing pipeline, meticulously designed to guide the data through three critical stages: (1) Signal Extraction and Image Conversion, where the transient physical event is captured and transformed into a graphical representation; (2) Image Preprocessing and Contour Isolation, which employs a cascade of filtering and morphological operations to distill a clean, analyzable signal contour from a noisy background; and (3) Peak Detection and Semantic Classification, where the algorithm quantifies key topographical features of the contour to infer and assign the final seeding status. The complete, end-to-end workflow of this algorithm is illustrated in Figure 3.

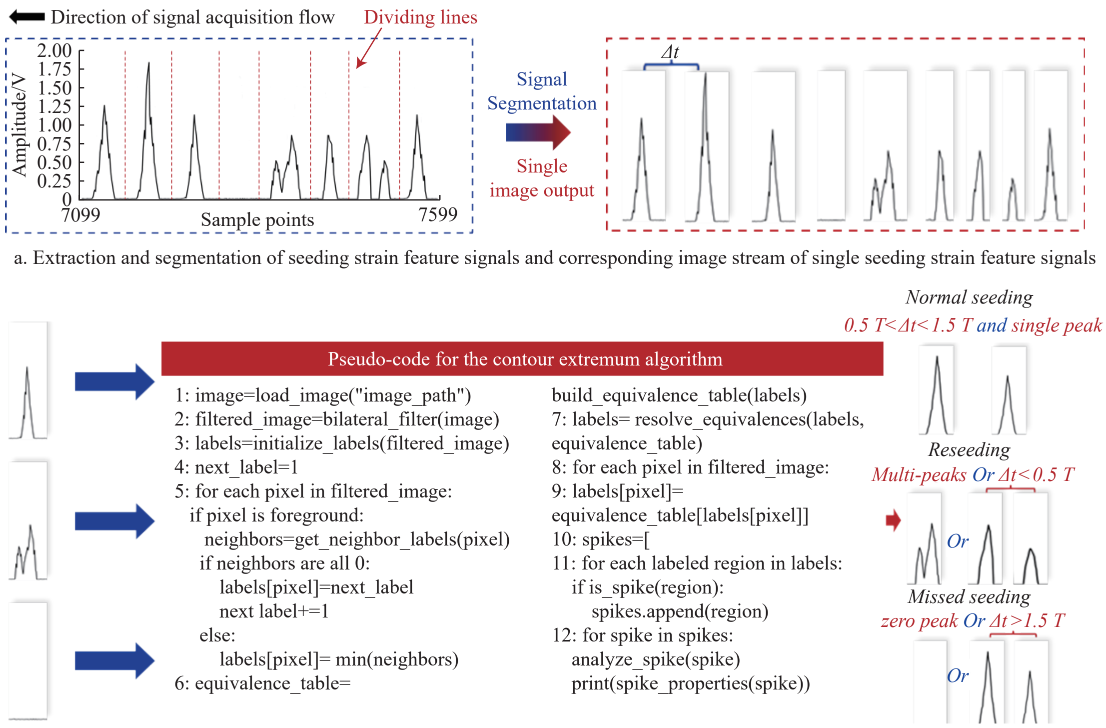

a. Extraction and segmentation of seeding strain feature signals and corresponding image stream of single seeding strain feature signals

b. Workflow of the SFIA algorithm

Figure 3 Working principle of the seeding signal strain feature recognition algorithm

2.2.1 Signal extraction and image conversion

The initial and most formidable challenge in any field-based sensing application is the robust differentiation of genuine target signals from pervasive background noise. In this context, noise manifests from two primary sources: high-frequency mechanical vibrations from the tractor and seeder chassis, and low-level electrical oscillations inherent to the data acquisition circuitry. To address this, the data acquisition module incorporates a simple yet effective front-end filter: a predefined signal amplitude threshold. The system remains dormant until the signal from the acquisition card surpasses this threshold, at which point it triggers the capture of a real-time data segment. This method effectively discards the majority of low-energy background noise at the source. The captured time-series data segment, representing a potential seeding event, is then programmatically plotted as a standard line graph. This graphical object is subsequently saved as a digital image file to a designated directory, thereby completing the crucial conversion of temporal data (pressure vs. time) into a spatial format (pixel intensity vs. position) for the subsequent image-based analysis pipeline (Figure 3a).

2.2.2 Image preprocessing and contour isolation

This stage is the most computationally intensive part of the SFIA, designed to methodically refine the raw signal image and isolate the singular, high-fidelity signal contour that is essential for robust analysis. The process involves four sequential and synergistic steps:

(1) Adaptive image binarization: To create a stark, high-contrast image that unambiguously separates the signal waveform from the background, we employ Otsu's method. This technique is particularly advantageous as it provides an unsupervised, adaptive

thresholding capability, eliminating the need for manual parameter tuning which would be impractical for a system deployed in variable field conditions. Otsu's algorithm operates by iterating through all possible threshold values and calculating the corresponding inter-class variance for the pixels partitioned into foreground (signal) and background classes (Equations (6)-(9)). The optimal threshold is the one that maximizes this variance, thus ensuring the most distinct separation between the two classes. The image is then converted into a pure binary format, with signal pixels rendered white and background pixels black.

$$p(i) = \frac{n_i}{N} \tag{6}$$

$$\begin{cases} \omega_0(t) = \sum_{i=0}^{t} p_i \\ \omega_1(t) = \sum_{i=t+1}^{L-1} p_i \\ \mu_0(t) = \sum_{i=o}^{t} i \cdot p(i)/\omega_0(t) \\ \mu_0(t) = \sum_{i=t+1}^{L-1} i \cdot p(i)/\omega_1(t) \end{cases} \tag{7}$$

$$\sigma_b^2(t) = \omega_0(t) \cdot \omega_1(t) \cdot \left[\mu_0(t) - \mu_1(t)\right]^2 \tag{8}$$

$$t* = \arg\max \sigma_b^2(t) \tag{9}$$

where, n_i represents the number of pixels with the grayscale intensity level i; N represents the total number of pixels in the image; L represents the total number of discrete gray levels (typically 256 for an 8-bit image).

(2) Morphological operations for feature integrity: The raw binary image, while high-contrast, may suffer from artifacts such as small gaps in the signal line or isolated noise pixels. To rectify these issues, a sequence of morphological operations is applied. Crucially, we utilize an anisotropic kernel (a rectangular structuring element of size [5, 3]) whose dimensions are intentionally biased to be wider than they are tall, mirroring the characteristic shape of the expected signal peaks. First, an image dilation operation is performed. This process effectively "thickens" the signal line, bridging any minor discontinuities in the peak contours. This is immediately followed by an erosion operation, which "thins" the features back to their approximate original size. By performing slightly more iterations of erosion than dilation, this two-step process (a morphological "opening") not only restores the feature's scale but also effectively removes extraneous noise pixels at the feature's edge, thereby ensuring the topological integrity and connectivity of the primary signal waveform.

(3) Contour segmentation and instancing: With a clean and contiguous binary feature, the next task is to formally identify it as a singular object. For this, the highly efficient Two-Pass algorithm is used to perform connected-component labeling. This algorithm systematically scans the image to identify all groups of adjacent foreground pixels, assigning a unique numerical label to each distinct connected region. This process robustly segments the primary signal waveform contour from any residual background noise or artifacts that may have survived the morphological operations. The resulting set of labeled contours is then partitioned using a sliding window approach (Equation 10) to isolate the signal corresponding to a single, complete seeding cycle, providing a discrete data instance for the final analysis stages (Figure 3a).

$$\begin{cases} N_x = \left[\frac{W - W_W}{S_x}\right] + 1 \\ N_y = \left[\frac{H - H_W}{S_y}\right] + 1 \end{cases} \tag{10}$$

where, W, H represent the width and height of the sliding window, respectively; S_x, S_y represent the step size (or stride) of the window in the horizontal and vertical directions; N_x, N_y represent the total number of window positions along the horizontal and vertical axes.

(4) Edge-Preserving Contour Smoothing: Although the extracted contour is now topologically clean, it may still possess minute, high-frequency fluctuations along its edge that could be erroneously detected as peaks. To mitigate this, a bilateral filter is applied to the single-channel binary image (Equation 11). This advanced filtering technique is superior to standard Gaussian blurs because it operates in two domains simultaneously. It considers not only the spatial proximity of pixels (penalizing distant pixels) but also their intensity similarity (penalizing pixels with different brightness values). This dual-weighting scheme allows it to intelligently smooth the contour line by averaging out small, abnormal fluctuations, while critically preserving the sharp, well-defined edges and textures of the true signal peaks. This final denoising step is paramount for enhancing the signal-to-noise ratio of the contour's geometry, thereby significantly improving the reliability of the subsequent peak detection module (Figure 3b).

$$B(x,y) = (1/W) * \sum \left[I(x+i, y+i) * w(i,j) * d(I(x+i, y+i), I(x,y))\right] \tag{11}$$

where, $B(x,y)$ represents the intensity of the output pixel at coordinates (x,y) after bilateral filtering; $I(x+i, y+j)$ represents the intensity of a neighboring pixel in the input (original) image; $w(i,j)$ represents the spatial domain weight, a Gaussian function of the geometric distance between the center pixel (x,y) and the neighboring pixel $(x+i, y+j)$; $d(I(x+i, y+j), I(x,y))$ represents the range (or tonal) domain weight, a Gaussian function of the difference in intensity between the center and neighboring pixels; W represents the normalization coefficient, ensuring that the sum of all weights equals one.

2.2.3 Peak detection and semantic classification

(1) Extrema Quantification via Gradient Analysis: The final, smoothed contour is now ready for quantitative analysis. The number of local extrema (peaks) is determined using a custom algorithm whose logic is analogous to the well-established Harris corner detector used in computer vision. For each pixel along the contour, image gradients in the horizontal (G_x) and vertical (G_y) directions are calculated (Equations (12) and (13)). These gradients describe the local intensity change and are used to construct a 2×2 structure matrix, K, for the local region (Equation (14)). This matrix summarizes the local gradient structure. A response value, R, is then calculated for each pixel based on the determinant and trace of its corresponding K matrix (Equation (15)). In this context, a large positive R value indicates a region of high curvature in both directions, which corresponds directly to a peak in our one-dimensional signal image. A pixel is therefore classified as a peak if its R value exceeds a carefully selected threshold Z, robustly identifying the key topographical features of the signal.

$$\begin{aligned} G_x = {} & \left[f(x+1,y-1) + 2*f(x+1,y) + f(x+1,y+1)\right] - \\ & \left[f(x-1,y-1) + 2*f(x-1,y) + f(x-1,y+1)\right] \end{aligned} \tag{12}$$

$$G_y = \left[f(x-1, y-1) + 2 * f(x, y-1) + f(x+1, y-1)\right] - \left[f(x-1, y+1) + 2 * f(x, y+1) + f(x+1, y+1)\right] \quad (13)$$

$$K = \sum_{x', y'} w(x'-x, y'-y) \begin{bmatrix} G_x^2 & G_x G_y \\ G_x G_y & G_y^2 \end{bmatrix} \quad (14)$$

$$R = \det(K) - a * tra^2(K) \quad (15)$$

where, $f(x, y)$ represents the pixel intensity or grayscale value at the spatial coordinates (x, y) within the image; G_x and G_y represent the image gradients in the horizontal (x-axis) and vertical (y-axis) directions, respectively. They quantify the rate of change in pixel intensity along each axis; x_i represents the i-th element of a given vector x; $w(x, y)$ represents the window function, which defines the local neighborhood or region of interest centered at coordinates (x, y) for analysis; $\det(K)$ represents the determinant of the structure matrix K, which is equivalent to the product of its eigenvalues ($\lambda_1 * \lambda_2$); $\mathrm{tr}(K)$ represents the trace of the structure matrix K, defined as the sum of its diagonal elements, which is also equivalent to the sum of its eigenvalues ($\lambda_1 + \lambda_2$).

(2) Seeding Status Classification Logic: The field seeding operation utilized a 2BYF-4 finger-clamp precision corn seeder. This machine employed a high-precision incremental photoelectric encoder (Omron Automation (China) Co., Ltd., type E6B2-CWZ6C, operating voltage: 5V, pulse count: 2000P/R) to collect real-time operational speed data. Speed information was transmitted in real time via an interface to the human-machine interface (Figure 4). This enables the calculation of the theoretical seeding interval T, establishing a baseline operational cadence. The final classification logic is then applied based on the number of peaks detected and the timing between events (Figure 3b): Normal seeding: An event is classified as a single, successful seeding if the corresponding signal image contains exactly one detected peak; Reseeding: An event is classified as a reseeding (i.e., multiple seeds) if either multiple distinct peaks are detected within a single signal image, or if multiple single-peak images are generated within one standard seeding time interval T; Missed seeding: An event is classified as a miss if the time elapsed since the last successfully classified event exceeds a safety margin of $1.5T$, or if a captured signal image is analyzed and found to contain zero detected peaks. This $1.5T$ factor provides a robust buffer against minor variations in seeder speed and mechanics.

a. Field experimental site diagram of S-SMS and P-SMS

b. Installation location of the S-SMS

c. Installation location of the P-SMS

Figure 4 Field experiment

2.3 Field comparative experiment of the seeding monitoring system

2.3.1 Trial site and tillage conditions

To evaluate the system's performance and robustness under realistic operational variability, field trials were conducted under two contrasting tillage conditions, representative of common agricultural practices. The first was a conventional tillage environment, characterized by a clean seedbed prepared post-harvest by clearing all corn stalks and roots, followed by standard cultivation. This represents an ideal, low-interference operating scenario. The second was a no-tillage environment, defined by the retention of shredded corn stalks on the soil surface from the previous season. Seeding was performed directly into this residue layer, representing a challenging, high-interference operating scenario with significant potential for dust and debris generation.

2.3.2 Experimental design: Factors and performance indicators

The field trials were designed to rigorously validate the performance of the proposed pressure-based monitoring system (S-SMS) against established benchmarks. The core of the experiment involved a direct comparison between three system configurations: our proposed S-SMS integrated with the novel Signal Feature Identification Algorithm (SFIA), and a conventional photoelectric sensor system (P-SMS) analyzed first with a basic Traditional Threshold Algorithm (TTA) and second with a more advanced Pulse Interval Algorithm (PIA). This comparison was conducted across a matrix of operational conditions, including four distinct operating speeds (6, 8, 10, and 12 km/h) and the two tillage regimes described previously. The performance of each configuration was quantified using four key evaluation indicators, with each combination of factors replicated five times. The formulas, corrected for sequential numbering, are as follows:

$$\eta_n = \frac{1}{15}\sum_{i=1}^{3}\sum_{j=1}^{5}\frac{|n_{ij} - n'_{ij}|}{n'_{ij}} \times 100\% \quad (16)$$

$$\eta_r = \frac{1}{15}\sum_{i=1}^{3}\sum_{j=1}^{5}\frac{|r_{ij} - r'_{ij}|}{r'_{ij}} \times 100\% \quad (17)$$

$$\eta_m = \frac{1}{15}\sum_{i=1}^{3}\sum_{j=1}^{5}\frac{|m_{ij} - m'_{ij}|}{m'_{ij}} \times 100\% \quad (18)$$

$$\eta'_m = 1 - \frac{1}{15}\sum_{i=1}^{3}\sum_{j=1}^{5}\frac{|m_{ij} - m'_{ij}|}{m'_{ij}} \times 100\% \quad (19)$$

where, for the j-th trial at the i-th speed level: η_t is the accuracy index for the total seed count. t_{ij} is the total number of seeds *monitored* by the system. t'_{ij} is the *actual* total number of seeds sown (ground truth). η_n is the accuracy index for single seeding events. n_{ij} is the number of single seeding events monitored by the system. n'_{ij} is the *actual* number of single seeding events. η_r is the accuracy index for reseeding events. r_{ij} is the number of reseeding events *detected* by the system. r'_{ij} is the *actual* number of reseeding events. η_m is the accuracy index for missed seeding events. m_{ij} is the number of missed seeding events *detected* by the system. m'_{ij} is the *actual* number of missed seeding events.

2.3.3 Experimental procedure and ground truth acquisition

The field trials were conducted from October 15 to October 30, 2023, at the experimental farm of the Harbin Academy of Agricultural Sciences (126°28′12″N, 45°51′52″E). The experimental platform consisted of a NEWHOLLAND 110-90 tractor providing power to a 2BYF-4 type finger-clamp no-tillage precision seeder, using Zhengdan 958 corn seeds (Figure 4a). To facilitate a direct, unbiased comparison and eliminate confounding variables, all three monitoring system configurations were mounted concurrently on the same seeder unit (Figures 4b and 4c). This parallel setup ensured that all systems were subjected to identical operational dynamics and environmental conditions during each experimental pass, allowing for a robust comparative analysis of their outputs. The "ground truth" data (i.e., the *actual* number of seeds sown, t'_{ij}, r'_{ij}, m'_{ij}), essential for calculating the performance indicators, was obtained by manually counting the seeds collected on a greased board of a specified length placed on the seedbed for each trial run.

2.3.4 Statistical analysis

All collected data were processed and analyzed using SPSS (Version 26.0, IBM Corp., Armonk, NY, USA) and OriginPro (Version 2021, OriginLab Corp., Northampton, MA, USA). An Analysis of Variance (ANOVA) was performed to determine if the experimental factors (monitoring system type, operating speed, tillage condition) had a statistically significant effect on the measured performance indicators. When the ANOVA indicated a significant effect at a confidence level of $p\leq0.01$, Fisher's Least Significant Difference (LSD) post-hoc test was employed to conduct pairwise comparisons between the different factor levels. This statistical approach allows for a robust determination of significant differences in performance between the tested systems. All data visualizations were generated using OriginPro.

3 Results and discussion

3.1 Performance under conventional tillage conditions

In the ideal, low-interference environment of conventional tillage, the proposed S-SMS with SFIA demonstrated statistically significant superiority over both benchmark systems across all performance indicators ($p\leq0.01$). Quantitatively, the SFIA configuration improved the total seeding accuracy index by 3.31% and 5.78% compared to the PIA and TTA configurations, respectively (Figure 5a). More critically, its accuracy in identifying reseeding and missed seeding events was enhanced by up to 6.61% and 8.89% (Figures 5b and 5c), while the overall monitoring error was reduced by as much as 4.56% (Figure 5d). With an average monitoring accuracy of 97.41% and specific detection accuracies for reseeding and missed seeding reaching 98.96% and 97.56%, the system comfortably exceeded national industry standards. This high level of performance, even in clean conditions, is primarily attributable to the inherent stability of the pressure-based sensing modality. The biomimetic, finger-clamp design ensures that each seed is conveyed with consistent force along a fixed trajectory. This creates a highly repeatable and distinct pressure signature for each seeding event, which the SFIA can reliably identify. Unlike photoelectric systems that can be affected by minor variations in seed trajectory or ambient light, the pressure-based system captures a direct mechanical signal, providing a more robust foundation for accurate monitoring from the outset.

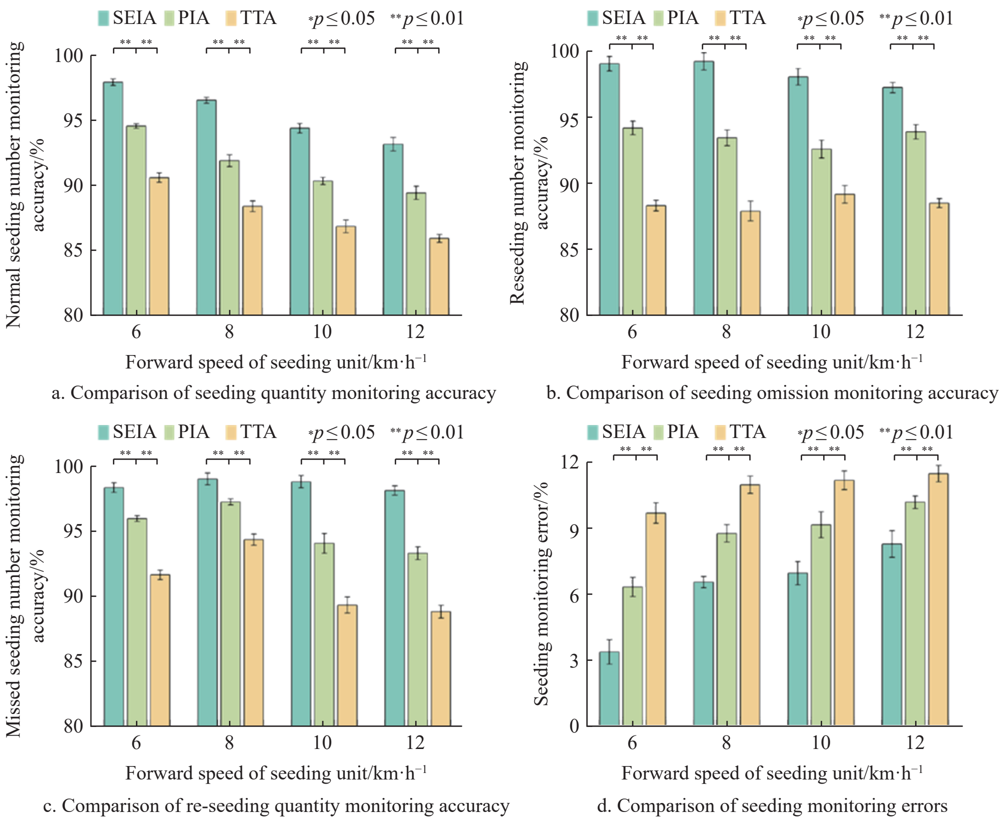

a. Comparison of seeding quantity monitoring accuracy b. Comparison of seeding omission monitoring accuracy

c. Comparison of re-seeding quantity monitoring accuracy d. Comparison of seeding monitoring errors

Figure 5 Conventional field trial results for SFIA, PIA, and TTA under different seeding speed conditions

3.2 Performance under challenging no-tillage conditions

The primary objective of the no-tillage trials was to evaluate the system's resilience in a high-interference environment, which represents a critical challenge for existing monitoring technologies. The results confirm that under these demanding conditions, the performance gap between the SFIA-based system and the photoelectric benchmarks widened considerably. The S-SMS with SFIA maintained its significant superiority ($p \leq 0.01$), improving the total seeding accuracy index by 3.92% and 7.66% over PIA and TTA, respectively (Figure 6a). The improvements in detecting reseeding and missed seeding events were even more pronounced, reaching up to 7.69% and 9.81% (Figures 6b and 6c), while the monitoring error was reduced by up to 6.28% (Figure 6d). Despite the challenging conditions, the system maintained an impressive overall accuracy of 97.25%. The discussion for this result is straightforward: the degradation in the performance of the photoelectric systems (P-SMS) is a direct consequence of the operational environment. No-tillage operations generate substantial amounts of dust and fine debris from crop residue. This airborne particulate matter inevitably enters the seed tube and coats the optical sensors, obstructing the light path and leading to frequent signal misinterpretations. The pressure-based S-SMS, being a mechanical contact-based system, is fundamentally impervious to such airborne contaminants. This immunity to dust interference is the core reason for its sustained high performance and its widening advantage in challenging field conditions.

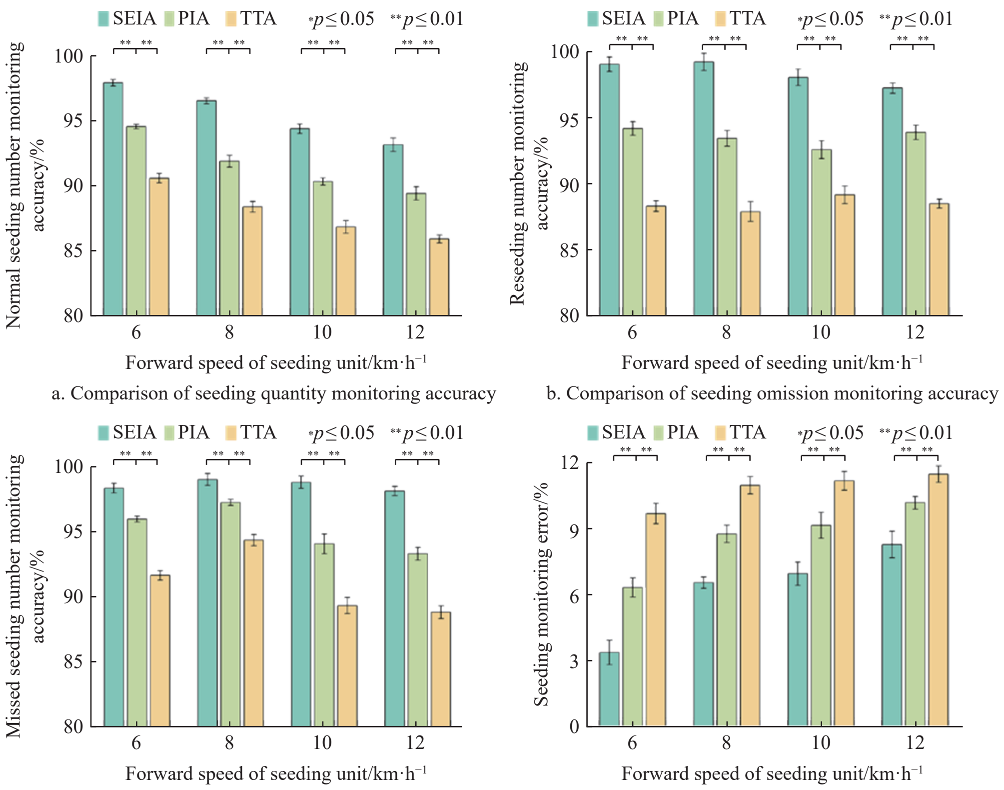

a. Comparison of seeding quantity monitoring accuracy
b. Comparison of seeding omission monitoring accuracy
c. Comparison of re-seeding quantity monitoring accuracy
d. Comparison of seeding monitoring errors

Figure 6 No-tillage field trial results for SFIA, PIA, and TTA under different seeding speed conditions

3.3 Overall performance comparison and discussion

Aggregating the data across all speeds and tillage conditions provides a definitive validation of the proposed system's superiority (Figure 7). Compared to the PIA and TTA benchmarks, the S-SMS with SFIA achieved an average improvement of 4.39% and 7.88% in total seeding accuracy, 3.63% and 7.56% in reseeding accuracy, and 2.97% and 6.58% in missed seeding accuracy, respectively. Concurrently, the overall monitoring error was reduced by 1.9% and 5.03%. These findings highlight a dual advantage of the pressure-based sensing approach combined with the SFIA. First, the inherent signal stability, derived from the consistent mechanical action of the finger-clamp seeder, provides a high-fidelity signal baseline that ensures superior accuracy even in ideal conditions. Second, and more importantly, the environmental resilience of the pressure sensor makes it robust against the primary failure mode of photoelectric systems—dust and debris contamination. It is this combination of inherent precision and operational robustness that establishes the proposed system as a significantly more reliable and effective solution for real-world precision agriculture applications.

3.4 Discussion

The superior performance of the pressure-based monitoring system (S-SMS) stems from two synergistic factors: the inherent stability of the signal source and its fundamental resilience to environmental interference. The biomimetic design of the finger-clamp mechanism is central to the first factor; it constrains each seed's movement, ensuring a consistent trajectory and force application upon the sensor. This mechanical consistency, largely insulated from chassis-level vibrations, generates a highly repeatable pressure signature for each seeding event. This clean, predictable signal provides an ideal input for the Signal Feature Identification Algorithm (SFIA), enabling reliable event classification even under optimal conditions.

This baseline advantage becomes critically important in challenging no-tillage environments, which highlights the second factor: environmental resilience. The high concentration of airborne dust and debris generated during no-tillage operations is the primary cause of failure for conventional optical systems. This particulate matter inevitably obstructs the light path of photoelectric sensors, leading to signal attenuation and frequent misclassifications. In stark contrast, the mechanical, contact-based principle of the S-SMS is fundamentally immune to these airborne contaminants. This immunity is the core reason for its sustained high accuracy and its widening performance gap over photoelectric systems in real-world, high-interference field conditions.

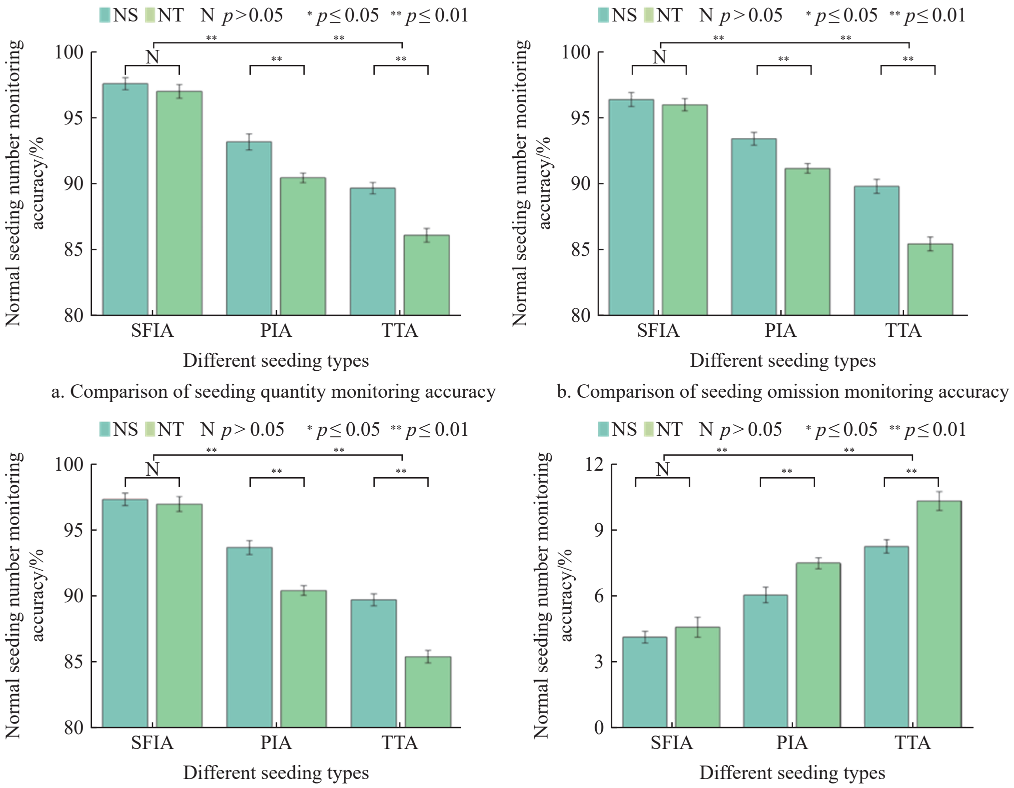

a. Comparison of seeding quantity monitoring accuracy
b. Comparison of seeding omission monitoring accuracy
c. Comparison of re-seeding quantity monitoring accuracy
d. Comparison of seeding monitoring errors

Figure 7 Results of conventional and no-tillage field trials for SFIA, PIA, and TTA across different seeding monitoring systems

4 Conclusions

This study successfully developed and validated a novel seeding monitoring system that integrates a flexible pressure sensor with a sophisticated Signal Feature Identification Algorithm (SFIA). In direct field comparisons against conventional photoelectric systems, the proposed system demonstrated markedly superior performance. It improved the total seeding accuracy index by up to 7.88%, reseeding detection accuracy by up to 7.56%, and missed seeding detection accuracy by up to 6.58%. Correspondingly, the overall monitoring error was reduced by as much as 5.03%. The primary driver of this enhanced performance is the system's robustness against environmental interference. Unlike photoelectric sensors, whose accuracy is significantly degraded by the dust and debris ubiquitous in field operations, the contact-based mechanical sensing principle is inherently resilient to such contaminants.

This research confirms that mechanical pressure signals represent a viable and robust alternative for high-fidelity seeding monitoring, particularly in challenging agricultural environments where optical methods falter. A current limitation is the system's specific optimization for finger-clamp seeders. Therefore, future work should focus on adapting the sensor integration and the SFIA to accommodate other prevalent seed metering mechanisms, thereby broadening the technology's applicability. Ultimately, this work underscores the critical importance of developing advanced, environmentally adaptive algorithms to unlock the full potential of next-generation agricultural sensing technologies.

Acknowledgements

This work is supported by the National Key Research and Development Program of China (2023YFD2301700), the Science and Technology Development Plan Project of Jilin Province (No. 20250601038RC), and the Science and Technology Development Project of Heilongjiang Beidahuang Land Reclamation Group Corporation.

[References]

[1] Qi J T, Jia H L, Li Y, Yu H B, Liu X H, Lan Y B, et al. Design and test of fault monitoring system for corn precision planter. Int J Agric & Biol Eng, 2015; 8(6): 13–19.

[2] Kim S J, Lee H S, Hwang S J, Kim J H, Jang M K, Nam J S. Development of seeding rate monitoring system applicable to a mechanical pot-seeding machine. Agriculture, 2023; 13(10): 2000.

[3] Zhang X Q, Li H S, Zhang S S. Design and analysis of laser photoelectric detection sensor. Microwave and Optical Technology Letters, 2021; 63(12): 3092–3099.

[4] Tao X, Lu H B, Luo W S. A robust photoelectric angular position sensor especially for a steerable underground boring tool. Sensors and Actuators a-Physical, 2005; 120(2): 311–316.

[5] Cleary T. Performance of dual photoelectric/ionization smoke alarms in full-scale fire tests. Fire Technology, 2010; 50(3): 753–773.

[6] Ding Z Q, Zhao Y, Zhang G L, Zhong M L, Guan X H, Zhang Y J. Application of visual mechanical signal detection and loading platform with super-resolution based on deep learning. International Journal of Intelligent Systems, 2022; 37(10): 7812–7836.

[7] Antoni J. Apports de la cyclostationnarité à l'analyse des signaux mécaniques. Mécanique & Industries, 2010; 11(1): 57–68.

[8] Arregi A, Lertxundi A, Vegas O, García-Baquero G, Ibarluzea J, Anabitarte A, et al. Environmental noise exposure and sleep habits among children in a cohort from Northern Spain. International Journal of Environmental Research and Public Health, 2022; 19(23): 16321.

[9] Gierz L, Paszkiewicz B K. PVDF piezoelectric sensors for seeds counting and coulter clogging detection in sowing process monitoring. Journal of

Engineering, 2020; 2020: 1–7.

[10] Li X, Li Y B, Tang C R, Li Y S. Modulation recognition network of multi-scale analysis with deep threshold noise elimination. Frontiers of Information Technology & Electronic Engineering, 2023; 24(5): 742–758.

[11] Nam H, Alouini M S. Effect of threshold quantization in opportunistic splitting algorithm. IEEE Communications Letters, 2011; 15(12): 1394–1397.

[12] Zhao Y, Chen Q, Cao W G, Yang J, Xiong J, Gui G. Deep learning for risk detection and trajectory tracking at construction sites. IEEE Access, 2019; 7: 30905–30912.

[13] Wang J, Chen X, Fang D, Wu C Q, Yang Z, Xing T. Transferring compressive-sensing-based device-free localization across target diversity. IEEE Transactions on Industrial Electronics, 2015; 62(4): 2397–2409.

[14] Dereich S, Vormoor C. The high resolution vector quantization problem with Orlicz norm distortion. Journal of Theoretical Probability, 2011; 24(2): 517–544.

[15] Zhao X, Gao Z M, Feng T, Shah S, Shi W D. Continuous fine-grained arm action recognition using motion spectrum mixture models. Electronics Letters, 2014; 50(22): 1633–1635.

[16] Fan H H, De P. High speed adaptive signal progressing using the delta operator. Digital Signal Processing, 2001; 11(1): 3–34.

[17] Li H G, Shi Y, Zhang B C, Wang Y F. Superpixel-based feature for aerial image scene recognition. Sensors, 2018; 18(1): 156.

[18] Wang H Z, Ma L. Image generation and recognition technology based on attention residual GAN. IEEE Access, 2023; 11: 61855–61865.

[19] Yu L. Application of infrared image detection based on high-resolution image processing in motion recognition. Optical and Quantum Electronics, 2024; 56(4): 615.

[20] Klemm O, Lange H. Trends of air pollution in the Fichtelgebirge mountains, Bavaria. Environmental Science and Pollution Research, 1999; 6(4): 193–199.

[21] Zhang W P, Zhao B, Gao S B, Ji Y X, Zhou L M, Niu K, Qiu Z M, Jin X. Online recognition of small vegetable seed sowing based on machine vision. IEEE Access, 2023; 11: 134331–134339.

[22] Wang Y, Jagota V, Makhatha M E, Kumar P. Vibration signal acquisition and computer simulation detection of mechanical equipment failure. Nonlinear Engineering, 2022; 11(1): 207–214.

[23] Xu F J, Jia T W, Jing R R. Recognition of key information in non-stationary signals based on wavelet threshold denoising and back propagation neural network optimized by manta ray foraging optimization algorithm. IEEE Access, 2022; 10: 118156–118166.

[24] Zhao J L, Wang X G, Wang J X, Han Z W. A high-precision strain seeding spacing monitoring system based on a combined bionic strain sensor and strain peak recognition algorithm. Computers and Electronics in Agriculture, 2023; 212: 108061.

[25] Tang H. Design and mechanism analysis of ripple surface pickup finger maize precision seed metering device. Doctoral Dissertation. Northeast Agricultural University, 2019.

[26] Ren J. Design and test of swinging finger clip corn seed-metering device. Master’s Thesis. Northeast Agricultural University, 2021.